

Prevailing features of X-ray induced molecular electron spectra revealed with fullerenes

Abraham Camacho Garibay, Ulf Saalmann, and Jan M. Rost
Max Planck Institute for the Physics of Complex Systems
 Nöthnitzer Straße 38, 01187 Dresden, Germany

Intense X-ray photo-absorption from short and intense pulses by a molecule triggers complicated electron and subsequently ion dynamics leading to photo-electron spectra which are difficult to interpret. Illuminating fullerenes offers a way to separate out the electron dynamics since the cage structure confines spatially the origin of photo and Auger electrons. Together with the sequential nature of the photo processes at intensities available at X-ray free electron lasers, this allows for a remarkably detailed interpretation of the photo-electron spectra as we will demonstrate. The general features derived can serve as a paradigm for less well-defined situations in other large molecules or clusters.

PACS numbers: 33.80.Wz, 79.77.+g, 81.05.ub, 41.60.Cr

An intense X-ray pulse as available from free-electron lasers [1, 2] triggers multiple electron emission from a large molecule. The resulting electron spectrum is quite complex since it contains photo electrons, Auger electrons and electrons evaporating from an almost thermalized nano-plasma cloud trapped by a positive background charge in the molecule, formed as a consequence of the many photo and Auger electrons leaving the system [3–6]. This charge is considerably larger than in synchrotron experiments [7] and along with the corresponding attractive potential depends on time. The latter builds up quickly with the departure of photo and Auger electrons while it becomes weaker upon expansion induced by ion-ion repulsion. The charging and the expansion of the ionic backbone crucially influences through this potential the electron spectrum since it determines the energy each individual electron carries after leaving the molecule, cf. Fig. 1.

In this situation it is very desirable to analyze a molecule which exhibits all the features described yet offers a chance for simplification due to its symmetry. An ideal candidate is the C_{60} fullerene which has sixty identical carbon atoms on a spherical shell such that each C-atom has the same distance to the molecular center. Moreover, fullerenes can be easily produced in the gas phase as well as in the form of powder samples in the crystalline phase providing an ideal target for experiments with free-electron laser beams. First intriguing femtosecond X-ray diffraction data of crystalline C_{60} have been obtained recently [8].

Here, we provide insight into the electron spectrum of C_{60} through a theoretical approach which step by step adds complications to the dynamics of the fullerene, ultimately providing a realistic spectrum whose features become then understandable as remnants of the artificially simplified dynamics introduced before. To this end we will first consider one photo electron (and accompanying Auger electron) per atom without trapping and plasma formation and discuss the different shapes of the spectrum obtained from rate equations as a function of the ratio of Auger rate γ and photo-ionization rate κ .

The ratio γ/κ can be varied by changing the intensity of the X-ray pulse. Of course, we keep all ions fixed for this synthetic spectrum. In a next step we provide the full electron spectrum of C_{60} for multi-channel ionization and Auger events determined by a molecular dynamics calculation, but still for fixed ions. In a final and last step we present full dynamical electron spectra including ion motion, starting from very short but realistic pulses (1 fs duration, 10^{19} W/cm² intensity) to make contact with the fixed-ion spectra. We will see that ion motion significantly changes the spectra for longer pulses (up to 15 fs). We have refrained from averaging our results over the laser focus for clarity and also, since in principle simultaneous imaging [9] of the targets may allow in the future to determine accurately under single-shot conditions the

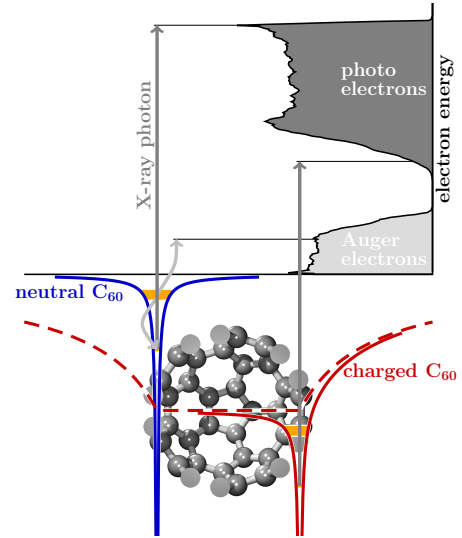


FIG. 1: Sketch of the formation of broad electron spectra. The highest energy is observed for photo-ionization of core electrons from neutral C_{60} (blue solid line on the left). For a charged C_{60} (red solid line on the right) the energy is reduced due to the background potential (red dashed line).

intensity with which the molecule was hit.

Dealing with X-rays of more than 1 keV, we will only consider the photo-ionization of the 1s carbon electrons [10]. We have checked that photo-ionization of electrons from the valence shell in C_{60} is in comparison negligible. They account for less than 5% of the total photo-absorption cross section. Auger processes are described on the basis of a molecular Auger lifetime of 6 fs, a typical value for carbon in molecular environment [11, 12]. Photo-absorption as well as Auger-decay processes are modeled with a Monte Carlo procedure. We include all possible transitions (ss, sp, pp) with branching ratios according to the atomic case [13] and the instantaneous valence-shell occupations [14]. Note that radiative decay (fluorescence) of Carbon core-holes in a molecular environment is about two orders of magnitude slower than non-radiative (Auger) decay [13].

The probability that an electron is emitted with energy E is given by an integral [15] over emission times $P(E) = \int dt p(t) \delta(E - E'(t))$ with $p(t)$ the ionization rate at time t and $E'(t)$ the final energy of an electron released at that time. The energy E' is time-dependent due to the formation of a background potential mentioned before and given explicitly in Eq. (2). Considering various ionization channels x , which will be specified below, and writing the ionization rate in terms of $n(t)$, the number of electrons released up to time t , the spectrum reads

$$P(E) = \sum_x \int dt \dot{n}_x(t) \delta(E - E'_x(t)) \quad (1a)$$

$$= \sum_x \left| \frac{\dot{n}_x(t)}{\dot{E}'_x(t)} \right|_{t=t'_x(E)} \quad (1b)$$

whereby Eq. (1b) follows from properties of the δ -function [15] with $t'_x(E)$ being the inverse function of $E'_x(t)$. Time derivatives are denoted with a dot. The final energies of the electrons depend on the charge of all other ions in the C_{60} at the instant of their creation. For the discussion it is convenient to consider an overall charge $Q(t)$ being homogeneously distributed over a sphere with radius $R(t)$. The corresponding potential is shown in Fig. 1 as dashed line. Thereby the final energies are

$$E_x(t) = E_x^* + V(t) \quad (2a)$$

$$V(t) = -\frac{Q(t)}{R(t)}, \quad Q(t) = \sum_x n_x(t), \quad (2b)$$

where E_x^* are the respective excess energies, which would be measured, if an electrons is released from channel x of a single carbon atom. The excess energies appear as characteristic energies in the spectrum

$$E_{ph}^* = E_\omega - B_0 \quad (3a)$$

$$E_{au}^* = A_1 \quad (3b)$$

$$E_{ph}^{\min} = E_\omega - B_{j_{\max}} - \tilde{Q}/R_0 \quad (3c)$$

with B_j the binding energies of the 1s core in C^{j+} and A_j the energies of the valence electrons released during the Auger decay α_j of a core-hole ion C^{j+} . Indeed there are various Auger decay channels with different energies for a certain charge state j . Since those differences are small on the energy scale considered here, we use in the discussion as A_j the average of those energies corresponding to α_j . The photo and Auger excess energies (3a,b) are “upper limits” and correspond to the respective atomic carbon lines. The third energy (3c) marks a “lower limit”. It is observed for the last photo electron which is released from $C^{j_{\max}+}$ and an overall charge $\tilde{Q} = Q(t \rightarrow \infty)$. Here and in the following we denote final variables with a tilde. As mentioned before, for the moment we neglect ionic motion and set $R(t) = R_0 = 3.52 \text{ \AA}$.

We consider in our first simple step only one photo electron per (fixed) atom in C_{60} and the subsequent Auger electron. This leads to the coupled rate equations for the time-dependent numbers of neutral atoms k , singly- and

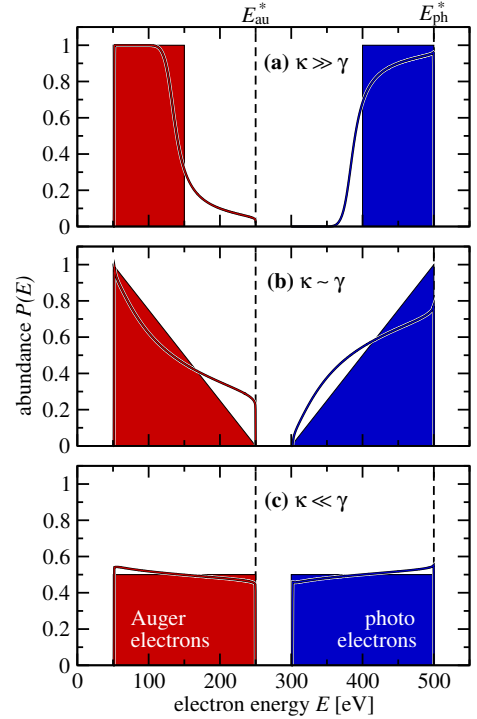


FIG. 2: Spectra for photo (blue) and Auger (red) electrons for three scenarios (a)–(c) corresponding to different ratios of photo-ionization rate κ to Auger rate ($\gamma=1$). From top to bottom $\bar{\kappa}/\gamma = 10, 1, 1/10$ with pulse durations $T = 2/\bar{\kappa} = 2/10, 2, 20$, respectively. The atomic excess energies of $E_{au}^*=250 \text{ eV}$ and $E_{ph}^*=500 \text{ eV}$ are marked by the dashed lines. Shaded areas mark the results for rectangular pulses, in (a) and (c) for the limiting case $\kappa \rightarrow \infty$ and $\gamma \rightarrow \infty$, respectively, in (b) for the special case of a fixed ratio $\kappa/\gamma = 2$.

doubly-charged ions k^+ and k^{++} ,

$$\dot{k}(t) = -\kappa(t) k(t) \quad (4a)$$

$$\dot{k}^+(t) = \kappa(t) k(t) - \gamma k^+(t) \quad (4b)$$

$$\dot{k}^{++}(t) = \gamma k^+(t). \quad (4c)$$

The initial conditions ($t \rightarrow -\infty$) for neutral C_{60} are $k=60$ and $k^+=k^{++}=0$. From the ion numbers follow the number of photo-electrons $\dot{n}_{ph}(t) = -\dot{k}(t)$ and of Auger electrons $\dot{n}_{au}(t) = \dot{k}^{++}(t)$.

To simplify things even more we consider first a rectangular pulse with a constant κ , which allows an explicit solution of the rate equations (4). The resulting spectrum is shown in Fig. 2 for $E_{ph}^* = 500$ eV and various ratios κ/γ . We have set $\gamma=1$ and chosen κ accordingly. The pulse duration T was adapted in order to absorb 25 photons, i.e., for $t \rightarrow +\infty$ it is $\tilde{n}_{ph} \approx 25$ and, of course, $\tilde{n}_{au} = \tilde{n}_{ph}$.

For very fast photo-ionization ($\kappa \rightarrow \infty$) all photo electrons produced by the laser pulse have escaped before the first Auger electron is emitted. Consequently, the last photo electron has to escape against a potential of $\tilde{V} \approx -100$ eV, which results from the positive charge of $\tilde{Q} = \tilde{n}_{ph}$ accumulated through photo-ionization. This explains the rectangular high-energy spectrum in Fig. 2a. Such plateau-like spectra have been seen [16] and explained [17] before for valence ionization of atomic clusters. Indeed their appearance is quite general [6, 18]. The final energy of the first Auger electron is reduced from $E_{au}^* = 250$ eV to $E_{au}^* - \tilde{V}$, while those of the last one is reduced by $2\tilde{V} \approx -200$ eV, since now the total positive charge is $\tilde{Q} = 2\tilde{n}_{ph}$. This explains the low-energy rectangular spectrum for energies $E = 50 \dots 150$ eV.

For the spectrum in Fig. 2c the Auger decays are instant ($\gamma \gg \kappa$). This means that in-between two photo-ionization events an Auger event takes place. Therefore, the background charge for the next photo electron increases by $\delta Q = 2$, stretching the interval of the photo-electron spectrum by a factor of 2 to energies $E = 300 \dots 500$ eV. The same is true for the Auger spectrum since each photo-electron is accompanied by an Auger electron. The overall shift of about 250 eV is due to a lower excess energy E_{au}^* .

Clearly, if both photo-ionization and Auger decays are decoupled due to very different rates, one expects flat spectra. This changes if both rates are similar. In particular for a fixed ratio $\kappa/\gamma = 2$, the electron spectrum takes a special form. In this case the spectra become triangular as shown in Fig. 2b. This particular shape can be obtained analytically from Eq. (1). The spectra with a time-dependent photo-ionization rate $\kappa(t) = \bar{\kappa} \sqrt{6/\pi} \exp(-(t/T)^2)$ following a realistic Gaussian pulse can be understood as deviations from the idealized shapes just discussed for constant photo-absorption in the three limiting cases of ratios κ/γ , cf. Figs. 2a–c. Here we compare the mean photo-ionization rate $\bar{\kappa}$ [19] with the Auger rate γ .

As a next step of complication we discuss the full electron spectrum for fixed ions resulting from many-channel electron dynamics including double core-hole and plasma formation for the scenarios (a) and (b) from Fig. 2 with Gaussian pulses delivering photons of $E_\omega = 2$ keV energy. Results have been obtained with a molecular dynamics propagation of released electrons and the parameters are chosen such that more than 200 photo electrons are produced to activate all subsequent channels down to photo-ionization of the ground state of C^{5+} with $B_5 = 476$ eV entering Eq. (3c). A quick glance on Fig. 3 reveals that E_{au}^* and E_{ph}^* are the same for both scenarios as expected.

In scenario (b) the photo-ionization rate is small enough that on average an Auger electron is produced after each photo electron. A characteristic step appears at energy $E_{trap} = E_\omega - B_0 - A_1 = 1476$ eV (see Fig. 3b) separating the high-energy part from the low-energy part in the photo-electron spectrum. In the former after each photo electron an Auger electron escapes increasing the background charge by $\delta Q = 2$ while in the latter the Auger electron is trapped such that $\delta Q = 1$. Trapping occurs if the background potential is deep enough such that $Q_{trap}/R = A_1 = 239$ eV, the kinetic energy of the Auger electron produced in the Auger decay of C^+ with a 1s hole. Consequently, $Q_{trap}/2 \approx 29$ is the number of escaped Auger electrons, provided this step at E_{trap} exists in the spectrum. With the 29 escaped Auger electrons and the 238 photo electrons we estimate from Eq. (3c) $E_{ph}^{min} = 440$ eV in good agreement with Fig. 3b.

The spectrum of scenario (a) with $\kappa \gg \gamma$ lacks E_{trap} , since fast photo-ionization builds up a large Q before Auger electrons are produced. Dominant photo-ionization early in the pulse is confirmed by the triangular shape of the photo electron spectrum at its blue edge ($E \lesssim E_{ph}^*$). It forms if exactly two channels contribute whose rate has the ratio 2. This is the case for photo-ionization of C and C^+ with a single core-hole without

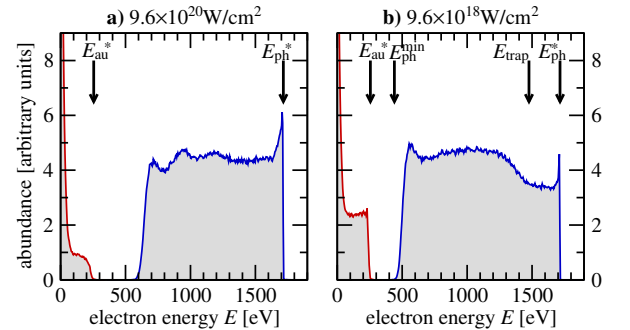


FIG. 3: Electron spectra for fixed ions generated with an X-ray pulse of 2 keV photons. The peak intensities are $9.6 \times 10^{20} \text{ W/cm}^2$ and $9.6 \times 10^{18} \text{ W/cm}^2$ for scenarios (a) and (b), respectively. From the area under the photo electron spectrum in the interval $[E_{ph}^{min}, E_{ph}^*]$ follows the number of photo electrons: $n_{ph}^{(b)} = 238, n_{ph}^{(a)} = 217$.

significant influence of other channels, e.g., Auger escape. Given that situation, we can read-off from Fig. 3a that $E_{\text{ph}}^{\text{min}} \approx 600 \text{ eV}$ and estimate with the help of Eq. (3c) and the 217 photo electrons that about 10 Auger electrons have escaped.

We are now in a position to understand the truly complex electron spectra resulting from full electron and ion dynamics when illuminated by an intense X-ray pulse of $E_{\omega} = 1.3 \text{ keV}$ photons. The highest intensities used are realistic, assuming 10^{13} photons per pulse focused onto $1 \mu\text{m}^2$ which gives roughly $I_{\text{max}} \approx (2/T_{\text{fs}}) \times 10^{20} \text{ W/cm}^2$. To make contact with the frozen ions discussed so far we consider first in Fig. 4 a $T = 1 \text{ fs}$ pulse. For weak intensity, i.e., only a few electrons ionized, the spectrum in Fig. 4a shows peaks slightly red-shifted to the atomic photo-electron and Auger-electron energies E_{ph}^* and E_{au}^* . For further increasing intensity the familiar *plateau* for the photo electrons develop due to the generation of background charge Q and for the same reason the Auger peak gets an increasing red-shift. As in Fig. 3 the energies $E_{\text{ph}}^{\text{min}}$ are consistent with the number of photo and Auger electrons which have escaped and the relevant excess energies B_j , cf. the figure caption. However, the Auger electrons reveal a new feature, namely the re-appearance of a peak close to the atomic line $A_3 = 224 \text{ eV}$ for high intensity, see Figs. 4c,d. The reason for this behavior is that the background potential Eq. (2b) is weak at early

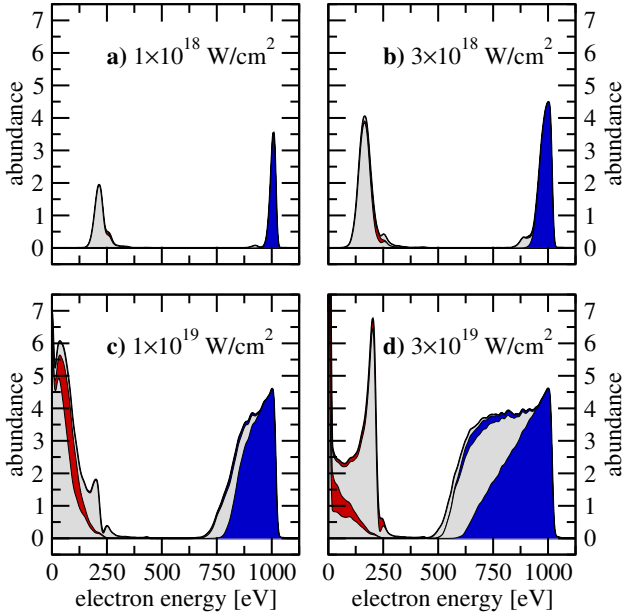


FIG. 4: (a-d) Electron energy spectra from C_{60} exposed to a short pulse ($T = 1 \text{ fs}$) of $E_{\omega} = 1.3 \text{ keV}$ photons for various intensities. Photo-electron contributions from C^{2j} are indicated in blue, for corresponding Auger electrons in red, and from all odd charged ions C^{2j+1} in grey. The area under the photo-electron spectra provides the number of photo electrons: $\{n_{\text{ph}}^{(a)}, n_{\text{ph}}^{(b)}, n_{\text{ph}}^{(c)}, n_{\text{ph}}^{(d)}\} = \{6, 17, 48, 98\}$.

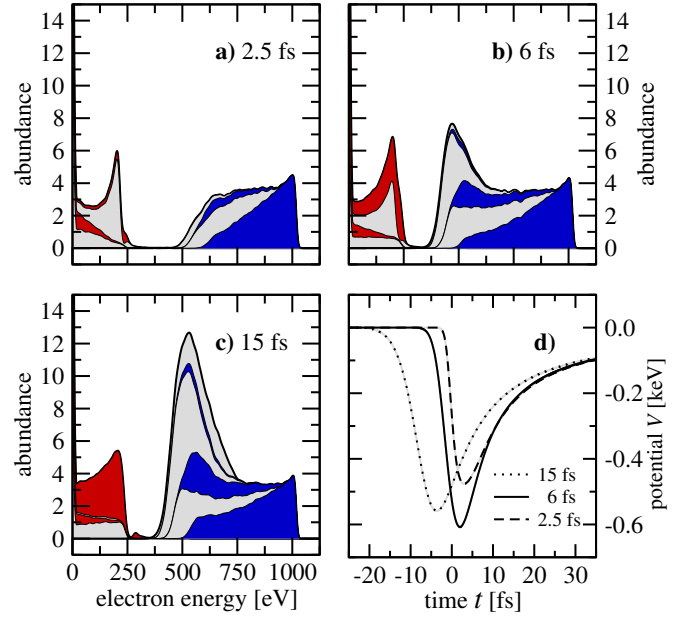


FIG. 5: (a-c) Electron energy spectra as in Fig. 4 but for a fixed peak intensity of $I = 10^{19} \text{ W/cm}^2$ and various pulse lengths T . Note that the spectrum for $T=1 \text{ fs}$ with the same intensity I is shown in Fig. 4c. Panel (d) shows the time dependent background potential $V(t)$, given by Eq. (2b), for the same pulse parameters. The number of photo electrons are $\{n_{\text{ph}}^{(a)}, n_{\text{ph}}^{(b)}, n_{\text{ph}}^{(c)}, n_{\text{ph}}^{(d)}\} = \{48, 96, 155, 208\}$.

and at late times when the fullerene is either weakly charged ($Q \approx 0$) or is exploded ($R \rightarrow \infty$), see Fig. 5d. Indeed, further analysis reveals that the α_3 -related peaks in Figs. 4c,d require a preceding Auger decay α_2 due to the short pulse (1 fs) which considerably delays the α_3 -decay.

The non-monotonic time dependence of the background potential together with the different emission times of the electrons can change the shape of the electron spectra qualitatively. This is further corroborated with Fig. 5a-c, where one sees drastic changes also in the photo-electron spectrum for longer pulses. The dominant effect is that electrons emitted late in or even after the laser pulse loose less and less energy turning the formation of a plateau into a pile up of electrons in a small energy interval, particularly striking for the (late) photo electrons from C^{j+} with $j > 2$ in Fig. 5c.

In summary we have analyzed the electron spectra of fullerenes following irradiation of short and intense X-ray pulses. These spectra reveal general features which will also allow one to interpret spectra of less symmetric large molecules. In particular triangular shapes will appear whenever two ionization channels are dominantly involved where one is twice as likely as the other, as it is the case with the photo-ionization of a filled ($1s^2$) and half-filled ($1s$) core shell. Moreover, we have established the onset $E_{\text{ph}}^{\text{min}}$ of the photo electron spectrum as characteristic energy which allows one to determine directly

the number of escaped Auger electrons in the case of C_{60} . Finally, peaks in the Auger spectra have to be interpreted carefully since they may not point to a unique decay process but to Auger electrons emitted from the molecule at rather different times with the same energy due to the non-monotonic change of the background potential. These features should prevail even if photon en-

ergies and Auger energies lead to overlapping photo and Auger electron spectra as well as post collision interaction, additional complications which will be investigated in future work.

This work was supported by the COST Action XLIC (CM 1204) and the Marie Curie Initial Training Network CORINF.

-
- [1] H. Chapman, J. Ullrich, and J. M. Rost, J. Phys. B **43**, 190201 (2010).
 - [2] P. Bucksbaum, T. Möller, and K. Ueda, J. Phys. B **46**, 160201 (2013).
 - [3] U. Saalmann and J. M. Rost, Phys. Rev. Lett. **89**, 143401 (2002).
 - [4] B. Ziaja *et al.*, New J. Phys. **11**, 103012 (2009).
 - [5] C. Bostedt *et al.*, New J. Phys. **12**, 083004 (2010).
 - [6] M. Arbeiter and T. Fennel, New J. Phys. **13**, 053022 (2011).
 - [7] R. C. Bilodeau *et al.*, Phys. Rev. Lett. **111**, 043003 (2013).
 - [8] B. Abbey *et al.*, arXiv:1209.5168 (2012).
 - [9] T. Gorkhover *et al.*, Phys. Rev. Lett. **108**, 245005 (2012).
 - [10] J. J. Yeh and I. Lindau, At. Data Nucl. Data Tables **32**, 1 (1985).
 - [11] T. X. Carroll *et al.*, Phys. Rev. A **61**, 042503 (2000).
 - [12] A. S. Schlachter *et al.*, J. Phys. B **37**, L103 (2004).
 - [13] E. Hartmann, J. Phys. B **21**, 1173 (1988).
 - [14] P. Di Cintio, U. Saalmann, and J.-M. Rost, Phys. Rev. Lett. **111**, 123401 (2013).
 - [15] J. M. Rost, Phys. Rep. **297**, 271 (1998).
 - [16] C. Bostedt *et al.*, Phys. Rev. Lett. **100**, 133401 (2008).
 - [17] C. Gnodtke, U. Saalmann, and J.-M. Rost, New J. Phys. **13**, 013028 (2011); Chem. Phys. **414**, 65 (2012).
 - [18] K. Moribayashi, Phys. Rev. A **80**, 025403 (2009).
 - [19] The mean photo-ionization rate is defined by requiring that the 0th and 2nd moment, $\int dt \kappa(t)$ and $\int dt t^2 \kappa(t)$, respectively, agree with the corresponding values for a rectangular pulse with a fixed photo-ionization rate, $\bar{\kappa}\bar{T}$ and $\bar{\kappa}\bar{T}^3/12$, respectively.